Journal of Medicinal Chemistry

Article

pubs.acs.org/jmc

Development of a Novel Class of Glucose Transporter Inhibitors

Dasheng Wang,[†,‡] Po-Chen Chu,[†,‡] Chia-Ning Yang,[§] Ribai Yan,[†] Yu-Chung Chuang,[§] Samuel K. Kulp,[†] and Ching-Shih Chen*[,†,∥]

[†]Division of Medicinal Chemistry, College of Pharmacy, The Ohio State University, Columbus, Ohio 43210, United States

[§]Institute of Biotechnology, National Kaohsiung University, Kaohsiung, Taiwan 811

[∥]Institute of Basic Medical Sciences, National Cheng-Kung University, 1 Ta-Hsueh Road, Tainan, 70101, Taiwan

ABSTRACT: On the basis of our finding that the antitumor effect of 5-{4-[(1-methylcyclohexyl)methoxy]benzyl}thiazolidine-2,4-dione, a thiazolidinedione peroxisome proliferator-activated receptor (PPAR)γ agonist, was, in part, attributable to its ability to block glucose uptake independently of PPARγ, we used its PPARγ-inactive analogue to develop a novel class of glucose transporter (GLUT) inhibitors. This lead optimization led to compound **30** {5-(4-hydroxy-3-trifluoromethylbenzylidene)-3-[4,4,4-trifluoro-2-methyl-2-(2,2,2-trifluoroethyl)butyl]thiazolidine-2,4-dione} as the optimal agent, which exhibited high antitumor potency through the suppression of glucose uptake (IC_{50}, 2.5 μM), while not cytotoxic to prostate and mammary epithelial cells. This glucose uptake inhibition was associated with the inhibition of GLUT1 (IC_{50}, 2 μM). Moreover, the mechanism of antitumor action of compound **30** was validated by its effect on a series of energy restriction-associated cellular responses. Homology modeling analysis suggests that the inhibitory effect of compound **30** on glucose entry was attributable to its ability to bind to the GLUT1 channel at a site distinct from that of glucose.

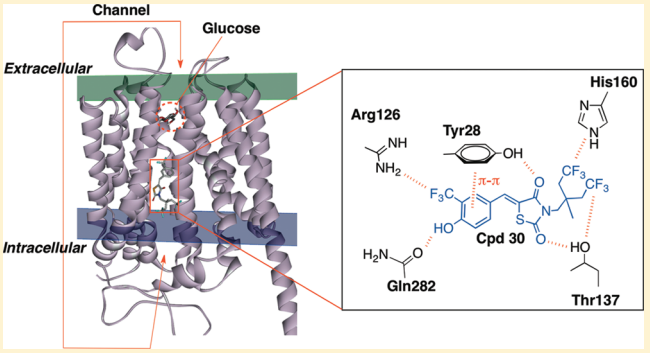

INTRODUCTION

Cancer cells gain growth advantages in the microenvironment by shifting cellular metabolism from oxidative phosphorylation to glycolysis, the so-called Warburg effect.[1−4] This glycolytic shift enables cancer cells to adapt to low-oxygen microenvironments, to generate biosynthetic building blocks for cell proliferation, to acidify the local environment to facilitate tumor invasion, and to generate NADPH and glutathione through the pentose phosphate shunt to increase resistance to oxidative stress.[2,5,6] Thus, the Warburg effect is considered as a fundamental property of neoplasia, thereby constituting the basis for tumor imaging by [^{18}F]2-fluoro-2-deoxyglucose positron emission tomography.[7] From a therapeutic perspective, targeting glycolysis by blocking glucose uptake represents a clinically relevant approach for cancer treatment, which has constituted the focus of many investigations.

Substantial evidence indicates that increased glucose uptake in malignant cells is associated with dysregulated expression of glucose transporter proteins, especially glucose transporter 1 (GLUT1).[8,9] GLUT1 is a class I facilitative sugar transporter responsible for basal glucose import required to maintain cellular respiration. GLUT1 overexpression has been reported in many types of human cancers, including those of brain,[10] breast,[11,12] cervix,[13] colon,[14] kidney,[15] lung,[16] ovary,[17] prostate,[18] thyroid,[19] and skin,[20] and is correlated with advanced cancer stages and poor clinical outcomes. This GLUT1 upregulation might be attributable to genetic alterations or environmental factors, including p53 mutations,[21] upregulated Akt signaling,[22] and hypoxia.[23] To date, a number of small-molecule agents capable of suppressing the activity/expression of GLUT1 and/or other GLUT members have been reported, including resveratrol,[24] naringenin,[25] phloretin,[26] fasentin,[27] 8-aminoadenosine,[28] and STF-31.[29] Exposure of cancer cells to these agents gave rise to reduced cell proliferation and/or chemosensitization, providing a proof-of-concept that targeting GLUT1 is a viable therapeutic strategy for cancer treatment.

Previously, we demonstrated that the suppressive effects of the peroxisome proliferator-activated receptor (PPAR)γ agonist 5-{4-[(1-methylcyclohexyl)methoxy]benzyl}thiazolidine-2,4-dione (**1**) on various signaling pathways, including those mediated by cyclin D1, Sp1, and androgen receptor (AR), in prostate cancer cells was attributable to its ability to block glucose entry independently of PPARγ.[30,31] This finding provides a mechanistic rationale for the present study of using the PPARγ-inactive analogues of **1** as a scaffold to develop a novel class of glucose transporter inhibitors. The proof-of-concept of this lead optimization was provided by compound **30**, which exhibited high potency in inducing apoptotic death in LNCaP cells through the suppression of glucose uptake (IC_{50}, 2.5 μM). Evidence suggests that this suppression of glucose entry was associated with the inhibition of GLUT1 (IC_{50}, 2 μM), the predominant

Received: January 4, 2012
Published: April 2, 2012

   dx.doi.org/10.1021/jm300015m | J. Med. Chem. 2012, 55, 3827−3836

GLUT isoform expressed in LNCaP cells. Moreover, the mechanism of antitumor action of compound **30** was validated by its ability to elicit a series of energy restriction-associated cellular responses, reminiscent of that of its parent compound.[30,31]

CHEMISTRY

Previously, we reported the pharmacological exploitation of the PPARγ-inactive analogue of compound **1**, (*Z*)-5-{4-[(1-methylcyclohexyl)methoxy]benzylidene}thiazolidine-2,4-dione (Δ2CG, **2**), as a scaffold to develop AR-ablative agents via its permuted isomer **3**, which led to (*Z*)-5-[4-hydroxy-3-(trifluoromethyl)benzylidene]-3-[(1-methylcyclohexyl)methyl]-thiazolidine-2,4-dione (CG-12, **4**) as the optimal compound (Figure 1A).[32] Our recent studies demonstrated that the suppressive effect of compound **4** on AR expression was associated with its ability to mimic glucose starvation through the inhibition of glucose uptake and the subsequent increase in the expression level of the E3 ligase β-transducin repeat-containing protein (β-TrCP).[30,31,33] This upregulation facilitated the proteasomal degradation of the transcription factor Sp1, leading to the transcriptional repression of AR. Thus, compound **4** was used as a starting point to generate potent glucose uptake inhibitors.

On the structural modification of compound **4**, we hypothesized that there exists interplay between the polar substituents on the phenyl ring and the terminal hydrophobic moiety in regulating its glucose uptake inhibitory activity. Accordingly, the methylcyclohexyl moiety of compound **4** was replaced by a series of hydrophobic moieties with varying degrees of bulkiness, generating compounds **5**−**9**, among which compound **5** exhibited the most potent suppressive effect on the uptake of [^{3}H]-2-deoxyglucose (2-DG) into LNCaP cells (Figure 2A).

Compound **5** was subjected to further modifications via three different strategies: (i) replacement of the electronegative -CF_3 function with various substituents (compounds **11**−**14**) or rearrangement of the disubstituents on the phenyl ring (compounds **15** and **16**), (ii) substitution at the 5-position with various functional groups (compounds **17**−**22**) or rearrangement of the trisubstituents on the phenyl ring (compounds **23**−**27**), and (iii) replacement of the terminal -CH_3 functions of the hydrophobic side arm with -CF_3 to enhance electronegativity (compound **28**) in conjunction with substitution of the tertiary proton with a F atom or -CH_3 group (compounds **29** and **30**, respectively). General procedures for the synthesis of these compounds are depicted in Figure 1B.

RESULTS

Screening of the Focused Compound Library to Identify Lead Glucose Uptake Inhibitors. The aforementioned derivatives (**5**−**30**) along with the parent compounds (**1**−**4**), each at 5 μM, were assessed for their abilities to block the uptake of [^{3}H]-2-DG into LNCaP cells after 30 min of exposure, which revealed a subtle structure−activity correlation (Figure 2A).

The role of the hydrophobic side chain in regulating the glucose uptake-inhibitory potency was manifested by the differential activities among compounds **4**−**9**, which showed an inverse correlation with the bulkiness of the hydrophobic moiety. Especially, the large discrepancy in inhibitory potency between compounds **5**−**8** and **4**/**9** underscored the preferential recognition of ligands with smaller hydrophobic side chains by target proteins. On the basis of this consideration, compound **5** was selected as the lead agent for further modifications.

Evidence indicates that the ligand binding entailed hydrophilic interactions with the polar substituents on the terminal phenyl ring. For example, masking of the -OH substituent of the terminal phenyl ring of compound **5** with a methyl group (compound **10**) abrogated the inhibitory activity. Moreover, the adjacent -CF_3 function could only be replaced with -NO_2 (**13**), but not -OH (**11**), -CH_3 (**12**), or -NH_2 (**14**), without compromising the drug activity, suggesting the involvement of electronegative function in protein−ligand interactions. This premise was also supported by lack of inhibitory activity in compounds **15** and **16**, both of which lacked an electronegative substituent on the phenyl ring.

Introduction of an additional electron-withdrawing group, such as -F (**17**), -Br (**18**), or -NO_2 (**21**), or a -OH function (**19**) on the 5-position led to a modest decrease in the glucose uptake activity compared to the parent compound **5**. However, substitution with -OCH_3 (**20**) or -NH_2 (**22**) resulted in a complete loss of activity. Compound **19**'s regioisomers, **23** and **24**, showed similar potency as their parent molecule, indicating flexibility in ligand recognition. This premise was supported by replacement of the -CF_3 of compound **23** with a -Br atom (**25**) which substantially reduced the inhibitory activity, but was contradicted by the similarity in the potencies of **24** and **26**. This discrepancy suggested the role of the catechol moiety of **26** in interacting with target protein(s), which was corroborated by the ability of its regioisomer **27** to block glucose uptake with similar potency. These catechols, however, were not amenable to drug development due to intrinsic chemical/metabolic instability.

Furthermore, compounds **18** and **21** are more acidic than the other derivatives examined, including **5**, **17**, **19**, **20**, and **22**, due to the inductive effect of the Br and NO_2 substituents ortho to the -OH group. By using a computational protocol in Discovery Studio 3.1, the pK_a values of these derivatives were calculated as follows: **5**, 8.0; **17**, 6.0; **18**, 6.6; **19**, 11.5; **20**, 9.6; **21**, 8.8; and **22**, 8.9. These pK_a values, however, did not show a correlation with the respective potencies of these compounds in suppressing glucose uptake, that is, **5** > **19** > **17**, **18** > **21** > **22**. This finding suggests that acidity of the phenolic moiety was not a primary determinant of the ligand binding.

Considering the enhancing effect of the CF_3 moiety on the activity and metabolic stability of drug candidates in the course of lead optimization,[34−36] we replaced the two terminal methyl functions at the hydrophobic side chain of compound **5** with CF_3 groups with or without substitution at the tertiary carbon, leading to **28**−**30**. All of these derivatives showed substantially improved potency relative to compound **5**, in the relative order **30** > **28** > **29**.

Furthermore, MTT assays indicated that the abilities of these thiazolidinedione derivatives to suppress the viability of LNCaP cells paralleled their respective inhibitory activities on glucose uptake (Figure 2B), suggesting a potential causal relationship between these two cellular events.

Suppression of Glucose Uptake through the Inhibition of Glucose Transporters. Dose−response analysis confirmed the high potency of compound **30** in blocking [^{3}H]-2-DG uptake into LNCaP cells with IC_{50} of 2.5 μM, while the IC_{50} values of other compounds examined were as follows: **28**, 3.5 μM; **5**, 6 μM; **4**, 9 μM; **2**, 52 μM; and **1**, 78 μM (Figure 3A). Glucose transport across the cytoplasmic membrane is mediated by members of the facilitative glucose transporter/solute carrier

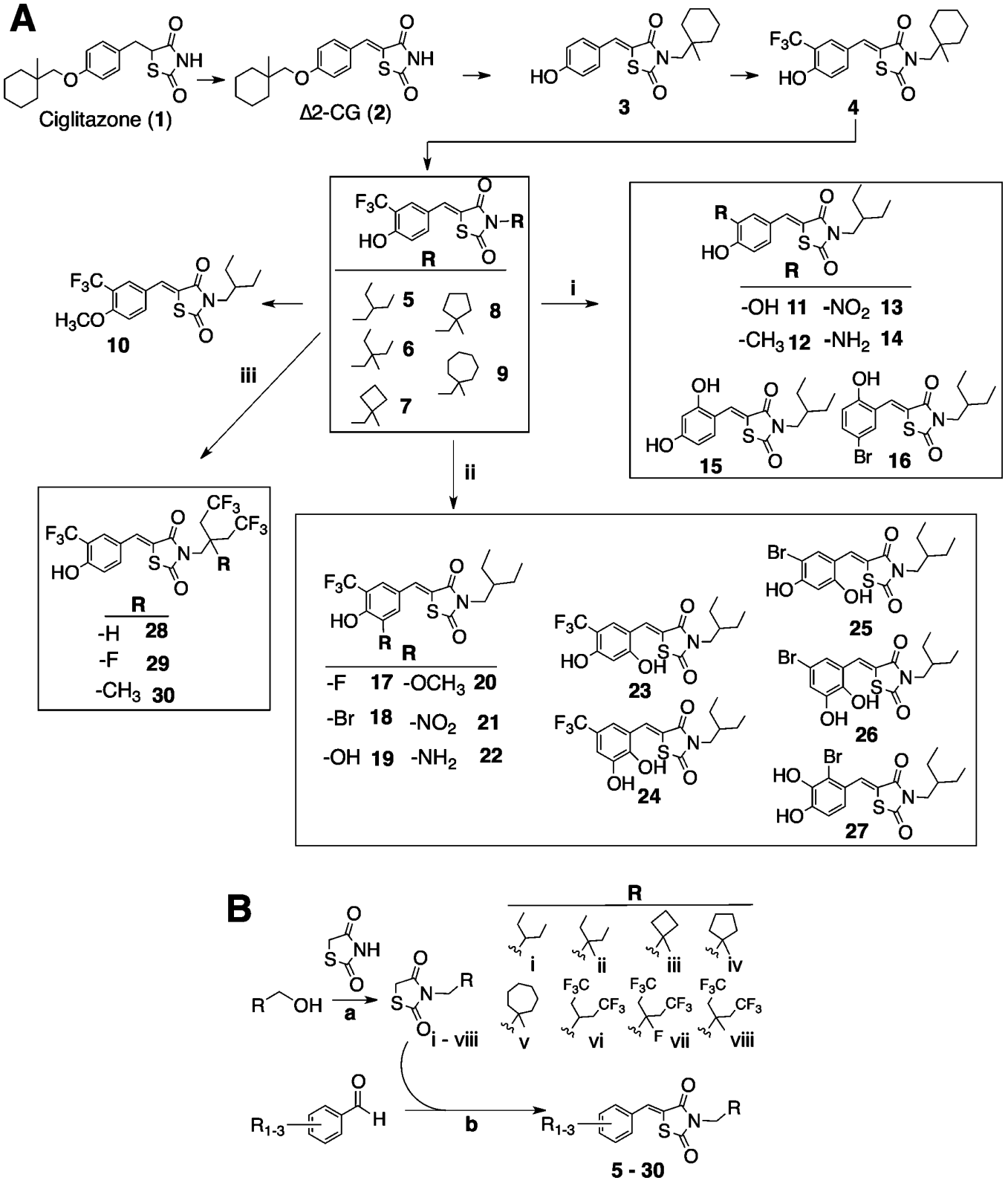

Figure 1. (A) Chemical structures of compounds **1**−**30** in the 5-{4-[(1-methylcyclohexyl)methoxy]benzyl}thiazolidine-2,4-dione-based focused compound library. (B) General synthetic procedure for compounds **5**−**30**. Reaction conditions: (a) DIPAD, TPP/dry THF; (b) piperidine, ethanol/reflux.

(GLUT/SLC2A) family.[37] To date, a total of 14 members have been identified, which are divided into three classes: class I, GLUT1−4 and GLUT14; class II, GLUT5, GLUT7, GLUT9, and GLUT11; class III, GLUT6, GLUT8, GLUT10, GLUT12, and H^+-coupled *myo*-inositol transporter.[37] As information regarding the expression patterns of individual GLUT members in LNCaP cells was lacking, we used quantitative real-time polymerase chain reaction to assess the mRNA levels of the

dx.doi.org/10.1021/jm300015m | *J. Med. Chem.* 2012, 55, 3827−3836

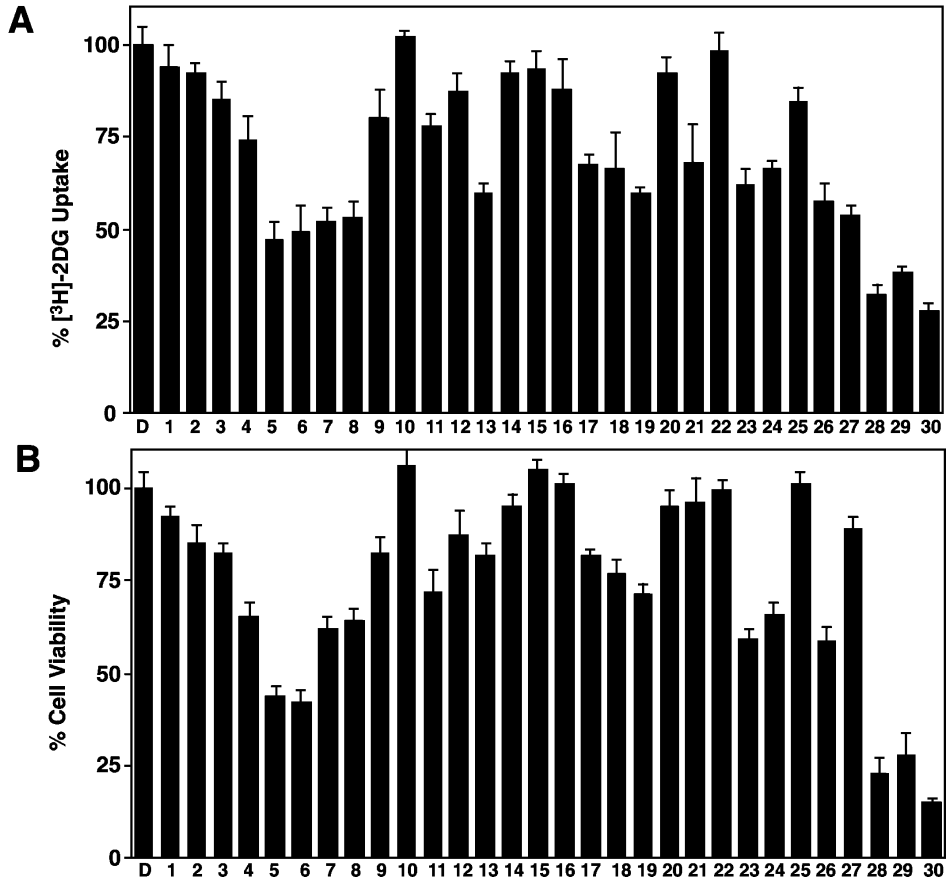

Figure 2. (A) Inhibitory effects of compounds **1**−**30**, each at 5 μM, on the uptake of [^{3}H]-2-DG into LNCaP cells in Krebs−Ringer phosphate buffer at 37 °C after 30 min of drug treatment. Column, mean; bars, SD (N = 3). (B) Corresponding effects of compounds **1**−**30** on the viability of LNCaP cells by MTT assays in 10% FBS-containing RPMI 1640 medium after 72 h of drug treatment. Column, mean; bars, SD (N = 6).

hypoxia-responsive GLUT1 and GLUT3 and three other representative GLUT members, including the class I GLUT2 and GLUT4 and the class II GLUT9. Among these five members, LNCaP cells expressed GLUT1 and, to a much lesser extent, GLUT9, while the mRNA levels of GLUT2−4 were negligible (Figure 3B).

To determine if the ability of compound **30** to inhibit glucose uptake in cancer cells could be attributed to the modulation of GLUT function, we examined the effects of **30** and its parent compound **5** on glucose uptake in LNCaP cells ectopically expressing GLUT isoforms. To assess the isoform specificities of the compounds, LNCaP cells were transfected with plasmids encoding GLUT1, GLUT3, GLUT4, or GLUT9 vis-à-vis the pCMV control vector so that the increased glucose uptake in GLUT-transfected cells relative to pCMV control cells was indicative of the activity of the ectopically expressed GLUT protein. Among the four GLUT members examined, GLUT1 was preferentially inhibited by compounds **5** and **30** at 5 μM (53% and 73%, respectively), followed by GLUT3 (41% and 48%, respectively), GLUT4 (32% and 42%, respectively), and GLUT9 (26% and 34%, respectively) (Figure 3C). The IC_{50} values for compounds **5** and **30** in inhibiting GLUT1-mediated [^{3}H]-2-DG uptake were 5 μM and 2 μM, respectively (Figure 3D), similar to those determined for suppression of glucose uptake in LNCaP cells (Figure 3A).

The high antiproliferative potency of compound **30** is associated with its ability to elicit energy restriction-associated cellular responses. Examinations of the dose-dependent suppressive effects of compounds **28** and **30** versus compounds **1**, **2**, **4**, and **5** on the viability of LNCaP cells revealed differential antiproliferative potencies that paralleled the respective inhibitory activities in glucose uptake (Figure 4A). After 72 h of exposure in 10% fetal bovine serum (FBS) -containing medium, the IC_{50} values for individual compounds were **30**, 1.5 μM; **28**, 2.2 μM; **5**, 4.2 μM; **4**, 6 μM; **2**, 28 μM; **1**, 60 μM. It is noteworthy that despite the high potency of the optimal agent compound **30** in suppressing the viability of LNCaP cells, normal human prostate epithelial cells (PrECs) and human mammary epithelial cells (HMECs) were resistant to the cytotoxic effect of compound **30** even at 10 μM (Figure 4B).

This drug-induced cell death was, at least in part, attributable to apoptosis, as evidenced by a dose-dependent increase in poly(ADP-ribose) polymerase (PARP) cleavage in response to compound **30** (Figure 4C). Equally important, compound **30** shared the reported activities of compound **4**, 2-DG, and glucose starvation in eliciting energy restriction-associated cellular responses in LNCaP cells, including β-TrCP-facilitated protein degradation, adenosine monophosphate-activated protein kinase (AMPK) activation, and endoplasmic reticulum (ER) stress.[30,38] Western blot analysis indicates that compound **30** dose-dependently increased β-TrCP expression, leading to the downregulated expression of its substrates cyclin D1 and Sp1, as well as the Sp1 target AR (Figure 4C). Furthermore, as AMPK negatively regulates the activation status of mammalian homologue of target of rapamycin (mTOR) and p70S6K signaling,[39] the drug-facilitated increases in AMPK phosphorylation

dx.doi.org/10.1021/jm300015m | J. Med. Chem. 2012, 55, 3827−3836

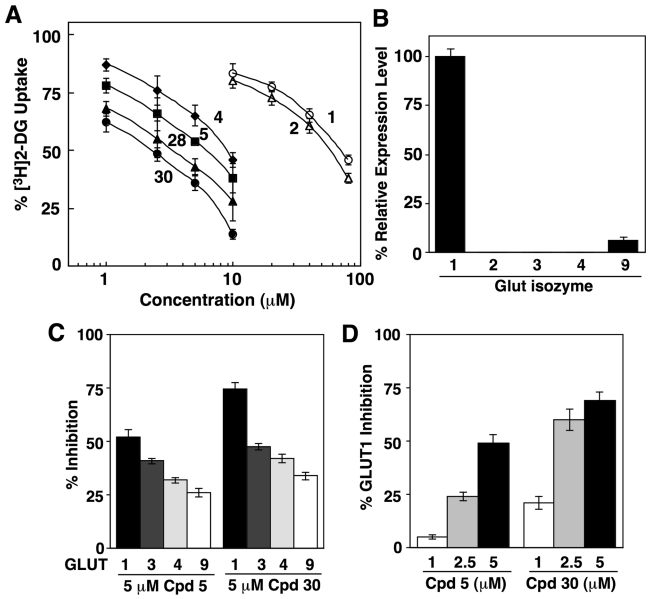

Figure 3. (A) Dose-dependent inhibitory effects of compounds **1**, **2**, **4**, **5**, **28**, and **30** on the uptake of [^{3}H]-2-DG into LNCaP cells in Krebs–Ringer phosphate buffer at 37 °C after 30 min of drug treatment. Points, mean; bars, SD (N = 3). (B) Quantitative real-time PCR analysis of the differential expression of GLUT1–4 and GLUT9 in LNCaP cells. Column, mean; bars, SD (N = 3). (C) Suppressive effects of compounds **5** and **30**, each at 5 μM, on [^{3}H]-2-DG uptake into LNCaP cells overexpressing GLUT1, GLUT3, GLUT4, or GLUT9. The analysis was carried out in Krebs–Ringer phosphate buffer at 37 °C after 30 min of drug treatment. Column, mean; bars, SD (N = 3). (D) Dose-dependent suppressive effects of compound **5** and **30** on [^{3}H]-2-DG uptake into LNCaP cells overexpressing GLUT1. Column, mean; bars, SD (N = 3).

was accompanied by concomitant decreases in the levels of p-mTOR and p-p70S6K. Compound **30**-induced ER stress was manifested by increased expression of two ER stress markers, glucose-regulated protein (GRP) 78 and growth arrest- and DNA damage-inducible gene (GADD) 153. Moreover, reminiscent of the demonstrated effect of compound **4** on the epigenetic activation of KLF6,[38] compound **30** increased the expression of this tumor suppressor protein in a dose-dependent manner.

Modeling Analysis of Ligand Binding. We also performed modeling analysis to envisage the mode of ligand binding using the homology-modeled structure of the human GLUT1 protein [Protein Data Bank (PDB) code 1SUK], which was developed by use of glycerol phosphate transporter as a template.[40] Blind docking simulations revealed that compound **30** and glucose bound to distinct sites in GLUT1's intermembrane channel for glucose passage (Figure 5A, left panel). While the glucose recognition site was located near the channel opening, compound **30** bound to the central segment of the channel. Docking analysis indicates that compound **30** interacted with the putative binding site through electrostatic and $\pi-\pi$ stacking interactions with Tyr^{28}, Arg^{126}, Thr^{137}, His^{160}, and Gln^{282}, as depicted in the close-up view (Figure 5A, right panel).

As compound **30** exhibits a calculated pK_a value of 8.0, the deprotonated form accounts for 13% of the total population of molecules in a physiological environment of pH 7.2. Therefore, we conducted another series of docking simulations to gain a better understanding of the interactions between the phenoxide and GLUT1's binding pocket. Compared to that shown in Figure 5A, the deprotonated form of compound **30** adopted a different mode of ligand binding such that the phenoxide moiety lay in close proximity to Arg^{126} to mediate ionic/hydrophilic interactions with its guanidine side chain (Figure 5B). Moreover, the amino hydrogen on the Trp^{412} side chain interacted with the sulfur atom and the carbonyl oxygen atom of the thiazolidinedione ring of compound **30**. In spite of the slightly upward shift in this binding mode, the $\pi-\pi$ interaction with Tyr^{28} and the electrostatic interaction of the terminal -CF_3 groups with His^{160} and Thr^{137} were maintained.

DISCUSSION

In the course of malignant transformation, tumor cells gain growth advantage by increasing glucose consumption through aerobic glycolysis.[1−4] This reprogramming of energy metabolism is manifested by increased glucose uptake through the upregulation of glucose transporters, especially GLUT1. In this study, we report the use of thiazolidinediones as a scaffold to develop a novel class of glucose transporter inhibitors. The optimal agent, compound **30**, exhibited high potency in suppressing the [^{3}H]-2-DG uptake and viability of LNCaP cells, with IC_{50} values of 2.5 μM and 1.5 μM, respectively, which represents a 40-fold improvement over that of compound **1**. Equally important, compound **30** exhibited no appreciable cytotoxicity in PrECs and HMECs, indicating the ability to discriminate between malignant and normal epithelial cells. Among the four GLUT isoforms examined, compound **30** preferentially inhibited GLUT1-mediated [^{3}H]-2-DG uptake with IC_{50} of 2 μM versus that of $\geq$5 μM for GLUT3, GLUT4, and GLUT9. The effectiveness of compound **30** in GLUT1 inhibition underlies its high potency in triggering energy restriction-associated cellular responses in LNCaP cells, leading to changes in the functional status of an array of signaling proteins governing cell cycle progression and apoptosis (Figure 6).

Docking modeling analysis suggests that the inhibitory effect of compound **30** on glucose entry is attributable to its ability to bind to the GLUT1 channel at a site distinct from that of glucose. This docking analysis provides a structural basis to account for the subtle structure–activity relationship among various derivatives of compound **5**. For example, compounds **28**–**30** exhibited higher potencies than compound **5** in GLUT1 inhibition, in part due to the additional electrostatic interactions of the two terminal -CF_3 functions with His^{160} and Thr^{137}. Similarly, relative to compounds **28** and **29**, the -CH_3 substituent on the tertiary carbon of compound **30** might have a steric effect on the configuration the two -CF_3 functions to allow closer interactions with His^{160} and Thr^{137} for tighter binding. Also noteworthy is the role of the -CF_3 function on the phenyl ring in mediating electrostatic interactions with Arg^{126}, which might account for the loss of glucose uptake inhibitory activity when this electronegative moiety in compound **5** was replaced by -CH_3 (compound **12**) or -NH_2 (compound **14**).

CONCLUSION

Data from this and other laboratories have demonstrated that targeting aerobic glycolysis via the inhibition of glucose transporters represents a therapeutically relevant strategy for cancer treatment. In light of the high potency of compound **30** in suppressing glucose uptake, it serves as a useful agent to shed light onto the signaling pathways, at both cellular and epigenetic levels, by which caloric restriction induces cancer cell

dx.doi.org/10.1021/jm300015m | J. Med. Chem. 2012, 55, 3827–3836

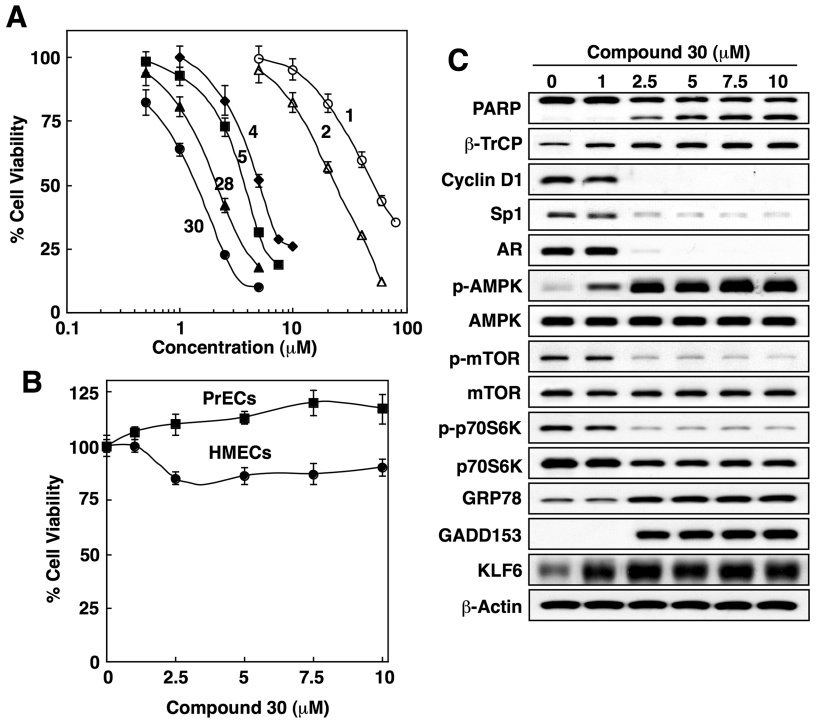

Figure 4. (A) Dose-dependent suppressive effects of compounds **1**, **2**, **4**, **5**, **28**, and **30** on the viability of LNCaP cells by MTT assays in 10% FBS-containing RPMI 1640 medium after 72 h of drug treatment. Points, mean; bars, SD ($N = 6$). (B) Dose-dependent effect of compound **30** on the viability of normal prostate epithelial cells (PrECs) and human mammary epithelial cells (HMECs) after 72 h of treatment. Points, mean; bars, SD ($N = 6$). (C) Western blot analysis of the dose-dependent effects of compound **30** on markers associated with apoptosis (PARP cleavage), β-TrCP-mediated protein degradation (β-TrCP, cyclin D1, Sp1, and AR), AMPK activation (p-AMPK, p-mTOR, and p-p706SK), ER stress (GRP78 and GADD153), and epigenetic activation of KLF6.

death through apoptosis and autophagy. From a translational perspective, research aimed at understanding these underlying mechanisms will help foster novel strategies for using this potent glucose transporter inhibitor, alone or in combination, in cancer therapy, which is currently underway.

EXPERIMENTAL SECTION

Unless otherwise indicated, all anhydrous solvents and chemical reagents were purchased at the highest grade available from Sigma–Aldrich (St. Louis, MO) and used without further purification. Flash column chromatography was performed with silica gel (230–400 mesh; Sorbent Technologies, Norcross, GA). Antibodies against various proteins were obtained from the following sources: Sp1, AR, cyclin D1, phospho-p70S6K (T389), p70S6K, GRP78, GADD153, and KLF6 were from Santa Cruz (Santa Cruz, CA); β-TrCP was from Invitrogen; phospho-Thr-172-AMPK, AMPK, phospho-Ser-2448-mTOR, mTOR, and PARP were from Cell Signaling Technology (Danvers, MA); and β-actin was from MP Biomedicals (Irvine, CA).

Nuclear magnetic resonance spectra (^{1}H NMR) were measured on a Bruker DPX 300 model spectrometer. Chemical shifts (δ) are reported in parts per million (ppm) relative to the tetramethylsilane (TMS) peak. Electrospray ionization mass spectrometric analyses were performed with a Micromass Q-Tof II high-resolution electrospray mass spectrometer. Melting points were determined by capillary melting point apparatus (Thomas-Hoover). The purity of all tested compounds was determined to be greater than 95% by elemental analyses, which were performed by Atlantic Microlab, Inc. (Norcross, GA) and were reported within 0.4% of calculated values. Compounds **2**–**4** were prepared as previously described.[32] General procedures for the synthesis of compounds **5**–**30** are depicted in Figure 1B.

Step a. To a mixture of individual alcohols (1.1 equiv), thiazolidine-2,4-dione (1.0 equiv), and triphenyl phosphine (3.5 equiv) in dry tetrahydrofuran (THF) was added diisopropyl azodicarboxylate (DIPAD; 3.3 equiv) dropwise at 0 °C. The reaction mixture was stirred at room temperature for 16 h, concentrated, dissolved in ethyl acetate, washed in tandem with water and brine, dried, and concentrated. The residue was purified by column chromatography (hexane/ethyl acetate) to afford N-substituted thiazolidine-2,4-diones (**i**–**viii**).

3-(2-Ethylbutyl)thiazolidine-2,4-dione ***(i)***. Light yellow oil; 81% yield. ^{1}H NMR ($CDCl_3$) δ 0.88 (t, J = 7.2 Hz, 6H), 1.28 (m, 4H), 1.70 (m, 1H), 3.51 (d, J = 7.2 Hz, 2H), 3.96 (s, 2H).

3-(2-Ethyl-2-methylbutyl)thiazolidine-2,4-dione ***(ii)***. Light yellow oil; 85% yield. ^{1}H NMR ($CDCl_3$) δ 0.81 (s, 3H), 0.86 (t, J = 7.2 Hz, 6H), 1.29 (m, 4H), 3.50 (s, 2H), 3.98 (s, 2H).

3-(1-Methylcyclobutylmethyl)thiazolidine-2,4-dione ***(iii)***. Light yellow oil; 80% yield. ^{1}H NMR ($CDCl_3$) δ 1.19 (s, 3H), 1.70 (m, 2H), 1.92 (m, 2H), 2.06 (m, 2H), 3.60 (s, 2H), 3.97 (s, 2H).

3-(1-Methylcyclopentylmethyl)thiazolidine-2,4-dione ***(iv)***. Light yellow oil; 81% yield. ^{1}H NMR ($CDCl_3$) δ 0.96 (s, 3H), 1.36 (m, 2H), 1.55 (m, 2H), 1.70 (m, 4H), 3.61 (s, 2H), 3.97 (s, 2H).

3-(1-Methylcycloheptylmethyl)thiazolidine-2,4-dione ***(v)***. Light yellow oil; 78% yield. ^{1}H NMR ($CDCl_3$) δ 0.93 (s, 3H), 1.36 (m, 2H), 1.54 (m, 10H), 3.60 (s, 2H), 3.97 (s, 2H).

3-[4,4,4-Trifluoro-2-(2,2,2-trifluoroethyl)butyl]thiazolidine-2,4-dione ***(vi)***. Light yellow oil; 82% yield. ^{1}H NMR ($CDCl_3$) δ 2.32 (m, 4H), 2.65 (m, 1H), 3.87 (d, J = 7.2 Hz, 2H), 4.05 (s, 2H).

3-[2,4,4,4-Tetrafluoro-2-(2,2,2-trifluoroethyl)butyl]thiazolidine-2,4-dione ***(vii)***. Light yellow oil; 81% yield. ^{1}H NMR ($CDCl_3$) δ 2.83–2.67 (m, 4H), 4.04 (d, J = 20.4 Hz, 2H), 4.07 (s, 2H).

3-[4,4,4-Trifluoro-2-methyl-2-(2,2,2-trifluoroethyl)butyl]-thiazolidine-2,4-dione ***(viii)***. Light yellow oil; 81% yield. ^{1}H NMR ($CDCl_3$) δ 1.19 (s, 3H), 2.47–2.25 (m, 4H), 3.77 (s, 2 H), 4.03 (s, 2H).

Step b. A mixture of individual di- and trisubstituted benzaldehydes (1.0 equiv), the corresponding N-substituted thiazolidine-2,4-dione (1.15 equiv), and a catalytic amount of piperidine in ethyl alcohol was refluxed until the reaction was completed, as monitored by thin-layer

dx.doi.org/10.1021/jm300015m | J. Med. Chem. 2012, 55, 3827–3836

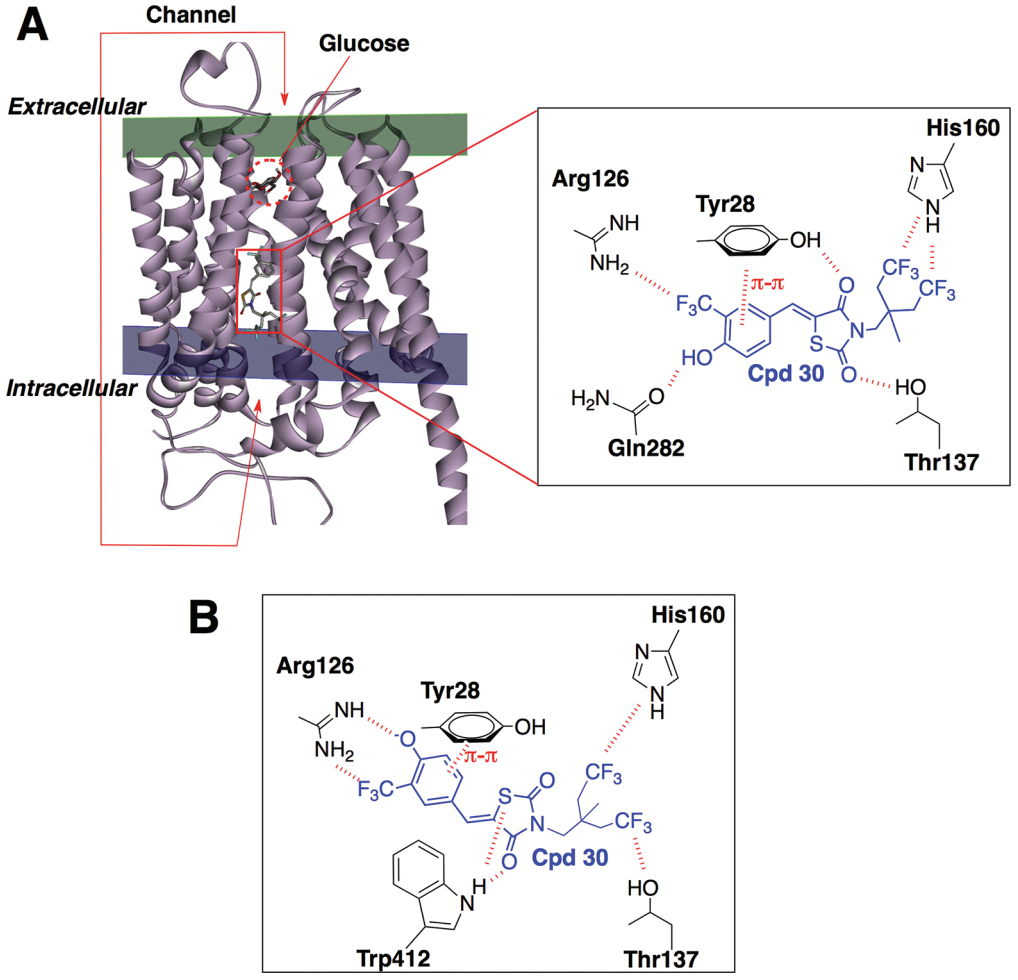

Figure 5. (A, left panel) Schematic representation of the predicted binding mode of compound **30** vis-à-vis that of glucose in the docking analysis of human GLUT1, showing that these two molecules bind to the transmembrane channel region at distinct sites. (A, right panel) Representation of the GLUT1 residues surrounding the docked compound **30**, showing the potential electrostatic and $\pi-\pi$ stacking interactions (dashed lines). (B) Representation of the GLUT1 residues surrounding the docked phenoxide species of compound **30**, showing the potential electrostatic and $\pi-\pi$ stacking interactions (dashed lines).

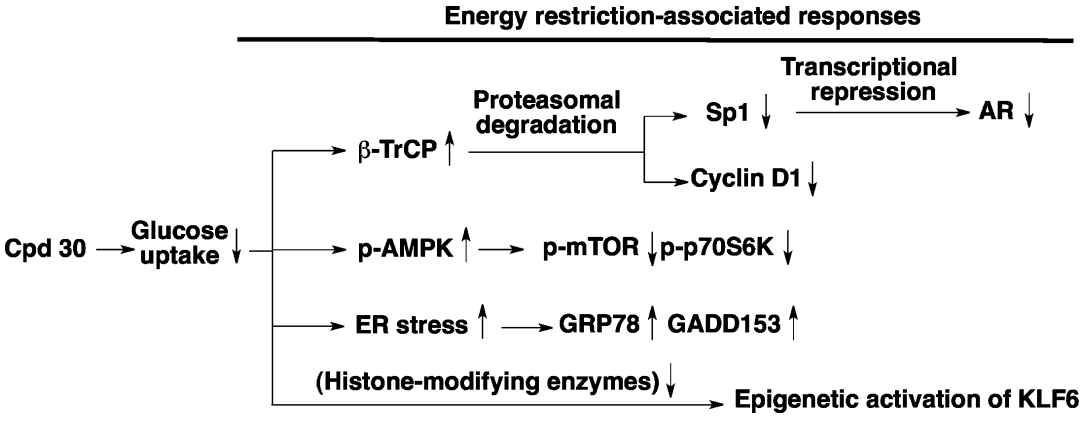

Figure 6. Schematic diagram depicting the mode of action of compound **30** in eliciting energy restriction-associated cellular responses.

chromatography (TLC), and concentrated. The residue was purified by column chromatography (hexane/ethyl acetate) to afford compounds **5**–**30**.

*3-(2-Ethylbutyl)-5-(4-hydroxy-3-trifluoromethylbenzylidene)-thiazolidine-2,4-dione (**5**).* White solid; 82% yield; mp 158–160 °C. ^{1}H NMR ($CDCl_3$) δ 0.92 (t, J = 7.2 Hz, 6H), 1.34 (m, 4H), 1.81 (m, 1H), 3.69 (d, J = 7.35 Hz, 2H), 6.19 (s, 1H), 7.10 (d, J = 8.58 Hz, 1H), 7.61 (d, J = 8.64 Hz, 1H), 7.70 (s, 1H), 7.83 (s, 1H). HRMS exact mass of $C_{17}H_{18}F_3NO_3S$ $(M + Na)^+$, 396.0857 amu; found, 396.0859 amu. Anal. Calcd, C 54.68, H 4.86, N 3.75; found, C 54.68, H 4.77, N 3.76.

*3-(2-Ethyl-2-methylbutyl)-5-(4-hydroxy-3-trifluoromethylbenzylidene)-thiazolidine-2,4-dione (**6**).* White solid; 78% yield. ^{1}H NMR ($CDCl_3$) δ 0.90 (m, 9H), 1.34 (m, 5H), 3.69 (s, 2H), 7.10 (d, J = 8.58 Hz, 1H), 7.55 (d, J = 8.64 Hz, 1H), 7.68 (s, 1H), 7.81 (s, 1H).

dx.doi.org/10.1021/jm300015m | J. Med. Chem. 2012, 55, 3827–3836

*5-(4-Hydroxy-3-trifluoromethylbenzylidene)-3-(1-methylcyclobutylmethyl)thiazolidine-2,4-dione (**7**).* White solid; 76% yield. ^{1}H NMR ($CDCl_3$) δ 1.19 (s, 3H), 1.86 (m, 4H), 2.08 (m, 2H), 3.78 (s, 2H), 6.21 (s, 1H), 7.11 (d, J = 6.6 Hz, 1H), 7.62 (d, *J* = 6.6 Hz, 1H), 7.71 (s, 1H), 7.85 (s, 1H).

*5-(4-Hydroxy-3-trifluoromethylbenzylidene)-3-(1-methylcyclopentylmethyl)thiazolidine-2,4-dione (**8**).* White solid; 80% yield. ^{1}H NMR ($CDCl_3$) δ 1.01 (s, 3H), 1.39 (m, 2H), 1.71 (m, 6H), 3.75 (s, 2H), 6.06 (s, 1H), 7.11 (d, *J* = 6.6 Hz, 1H), 7.62 (d, *J* = 6.0 Hz, 1H), 7.70 (s, 1H), 7.84 (s, 1H).

*5-(4-Hydroxy-3-trifluoromethylbenzylidene)-3-(1-methylcycloheptylmethyl)thiazolidine-2,4-dione (**9**).* White solid; 75% yield. ^{1}H NMR ($CDCl_3$) δ 0.93 (s, 3H), 1.38 (m, 2H), 1.54 (m, 10H), 3.75 (s, 2H), 6.08 (s, 1H), 7.11 (d, *J* = 6.6 Hz, 1H), 7.63 (d, *J* = 6.0 Hz, 1H), 7.70 (s, 1H), 7.86 (s, 1H).

*3-(2-Ethylbutyl)-5-(4-methoxy-3-trifluoromethylbenzylidene)-thiazolidine-2,4-dione (**10**).* White solid; 88% yield. ^{1}H NMR ($CDCl_3$) δ 0.92 (t, *J* = 7.2 Hz, 6H), 1.34 (m, 4H), 1.81 (m, 1H), 3.69 (d, *J* = 7.35 Hz, 2H), 4.02 (s, 3H), 7.10 (d, *J* = 8.58 Hz, 1H), 7.61 (d, *J* = 8.64 Hz, 1H), 7.70 (s, 1H), 7.83 (s, 1H).

*5-(3,4-Dihydroxybenzylidene)-3-(2-ethylbutyl)thiazolidine-2,4-dione (**11**).* Light brown solid; 80% yield. ^{1}H NMR ($CDCl_3$) δ 0.94 (t, *J* = 7.5 Hz, 6H), 1.34 (m, 4H), 1.81 (m, 1H), 3.68 (d, *J* = 7.2 Hz, 2H), 5.15 (s, 1H), 5.26 (s, 1H), 7.07 (d, *J* = 6.6 Hz, 1H), 7.10 (s, 1H), 7.18 (d, *J* = 8.58 Hz, 1H), 8.14 (s, 1H).

*3-(2-Ethylbutyl)-5-(4-hydroxy-3-methylbenzylidene)thiazolidine-2,4-dione (**12**).* White solid; 86% yield. ^{1}H NMR ($CDCl_3$) δ 0.92 (t, *J* = 7.2 Hz, 6H), 1.34 (m, 4H), 1.81 (m, 1H), 2.21 (s, 3H), 3.69 (d, *J* = 7.35 Hz, 2H), 6.19 (s, 1H), 7.10 (d, *J* = 8.58 Hz, 1H), 7.61 (d, *J* = 8.64 Hz, 1H), 7.70 (s, 1H), 7.83 (s, 1H).

*3-(2-Ethylbutyl)-5-(4-hydroxy-3-nitrobenzylidene)thiazolidine-2,4-dione (**13**).* Yellow solid; 73% yield. ^{1}H NMR ($CDCl_3$) δ 0.93 (t, *J* = 5.4 Hz, 6H), 1.35 (m, 4H), 1.80 (m, 1H), 3.67 (d, *J* = 5.4 Hz, 2H), 5.21 (s, 1H), 7.27 (d, *J* = 6.6 Hz, 1H), 7.32 (d, *J* = 6.8 Hz, 1H), 7.68 (s, 1H), 8.52 (s, 1H).

*5-(3-Amino-4-hydroxybenzylidene)-3-(2-ethylbutyl)thiazolidine-2,4-dione (**14**).* Brown solid; 68% yield. ^{1}H NMR ($CDCl_3$) δ 0.93 (t, *J* = 5.4 Hz, 6H), 1.35 (m, 4H), 1.80 (m, 1H), 2.26 (s, 2H), 3.67 (d, *J* = 5.4 Hz, 2H), 6.97 (d, *J* = 6.6 Hz, 1H), 7.22 (d, *J* = 6.8 Hz, 1H), 7.69 (br s, 1H), 7.87 (s, 1H), 8.76 (s, 1H).

*5-(2,4-Dihydroxybenzylidene)-3-(2-ethylbutyl)thiazolidine-2,4-dione (**15**).* Light yellow solid; 78% yield. ^{1}H NMR ($CDCl_3$) δ 0.93 (t, *J* = 7.5 Hz, 6H), 1.35 (m, 4H), 1.81 (m, 1H), 3.67 (d, *J* = 7.6 Hz, 2H), 6.52 (s, 1H), 6.60 (s, 1H), 6.76 (d, *J* = 6.6 Hz, 1H), 7.18 (d, *J* = 6.8 Hz, 1H), 7.54 (s, 1H), 8.14 (s, 1H).

*5-(5-Bromo-2-hydroxybenzylidene)-3-(2-ethylbutyl)thiazolidine-2,4-dione (**16**).* Light yellow solid; 84% yield. ^{1}H NMR ($CDCl_3$) δ 0.93 (t, *J* = 7.5 Hz, 6H), 1.35 (m, 4H), 1.81 (m, 1H), 3.67 (d, *J* = 7.6 Hz, 2H), 6.52 (s, 1H), 7.09 (d, *J* = 6.8 Hz, 1H), 7.21 (d, *J* = 6.6 Hz, 1H), 7.54 (s, 1H), 8.14 (s, 1H).

*3-(2-Ethylbutyl)-5-(3-fluoro-4-hydroxy-5-trifluoromethylbenzylidene)-thiazolidine-2,4-dione (**17**).* White solid; 81% yield. ^{1}H NMR ($CDCl_3$) δ 0.92 (t, *J* = 7.5 Hz, 6H), 1.34 (m, 4H), 1.80 (m, 1H), 3.68 (d, *J* = 7.2 Hz, 2H), 6.35 (br s, 1H), 7.46 (d, *J* = 10.8 Hz, 1H), 7.52 (s, 1H), 7.76 (s, 1H).

*3-(2-Ethylbutyl)-5-(3-bromo-4-hydroxy-5-trifluoromethylbenzylidene)-thiazolidine-2,4-dione (**18**).* Light yellow solid; 79% yield. ^{1}H NMR ($CDCl_3$) δ 0.91 (t, *J* = 7.5 Hz, 6H), 1.34 (m, 4H), 1.84 (m, 1H), 3.67 (d, *J* = 6.0 Hz, 2H), 6.05 (br s, 1H), 7.68 (d, *J* = 10.8 Hz, 1H), 7.76 (s, 1H), 7.82 (s, 1H).

*5-(3,4-Dihydroxy-5-trifluoromethylbenzylidene)-3-(2-ethylbutyl)-thiazolidine-2,4-dione (**19**).* Light brown solid; 76% yield. ^{1}H NMR ($CDCl_3$) δ 0.91 (t, *J* = 7.4 Hz, 6H), 1.34 (m, 4H), 1.84 (m, 1H), 3.67 (d, *J* = 8.4 Hz, 2H), 6.48 (br s, 1H), 6.53 (s, 1H), 7.18 (s, 1H), 7.35 (s, 1H), 7.81 (s, 1H).

*3-(2-Ethylbutyl)-5-(4-hydroxy-3-methoxy-5-trifluoromethylbenzylidene)-thiazolidine-2,4-dione (**20**).* White solid; 86% yield. ^{1}H NMR ($CDCl_3$) δ 0.91 (t, *J* = 7.4 Hz, 6H), 1.34 (m, 4H), 1.84 (m, 1H), 3.67 (d, *J* = 8.4 Hz, 2H), 4.05 (s, 3H), 6.48 (br s, 1H), 7.16 (s, 1H), 7.35 (s, 1H), 7.81 (s, 1H).

*3-(2-Ethylbutyl)-5-(4-hydroxy-3-nitro-5-trifluoromethylbenzylidene)-thiazolidine-2,4-dione (**21**).* Yellow solid; 75% yield. ^{1}H NMR ($CDCl_3$) δ0.91 (t, *J* = 7.4 Hz, 6H), 1.30 (m, 4H), 1.84 (m, 1H), 3.70 (d, *J* = 7.5 Hz, 2H), 5.69 (s, 1H), 7.81 (s, 1H), 8.05 (s, 1H), 8.48 (s, 1H).

*5-(3-Amino-4-hydroxy-5-trifluoromethylbenzylidene)-3-(2-ethylbutyl)thiazolidine-2,4-dione (**22**).* Brown solid; 70% yield. ^{1}H NMR ($CDCl_3$) δ 0.93 (t, *J* = 7.5 Hz, 6H), 1.35 (m, 4H), 1.81 (m, 1H), 2.36 (s, 2H), 3.67 (d, *J* = 7.2 Hz, 2H), 7.36 (s, 1H), 7.57 (s, 1H), 7.74 (s, 1H), 8.53 (s, 1H).

*5-(2,4-Dihydroxy-5-trifluoromethylbenzylidene)-3-(2-ethylbutyl)-thiazolidine-2,4-dione (**23**).* Off-white solid; 78% yield. ^{1}H NMR ($CDCl_3$) δ 0.93 (t, *J* = 7.5 Hz, 6H), 1.35 (m, 4H), 1.81 (m, 1H), 3.68 (d, *J* = 5.4 Hz, 2H), 6.32 (s, 1H), 6.56 (s, 1H), 7.20 (s, 1H), 7.68 (s, 1H), 8.26 (s, 1H).

*5-(2,3-Dihydroxy-5-trifluoromethylbenzylidene)-3-(2-ethylbutyl)-thiazolidine-2,4-dione (**24**).* Light brown solid; 74% yield. ^{1}H NMR ($CDCl_3$) δ 0.92 (t, *J* = 7.5 Hz, 6H), 1.33 (m, 4H), 1.79 (m, 1H), 3.67 (d, *J* = 7.2 Hz, 2H), 6.26 (br s, 2H), 7.21 (s, 1H), 7.30 (s, 1H), 8.12 (s, 1H).

*5-(5-Bromo-2,4-dihydroxybenzylidene)-3-(2-ethylbutyl)-thiazolidine-2,4-dione (**25**).* Off-white solid; 76% yield. ^{1}H NMR ($CDCl_3$) δ 0.93 (t, *J* = 7.5 Hz, 6H), 1.35 (m, 4H), 1.81 (m, 1H), 3.67 (d, *J* = 7.6 Hz, 2H), 6.52 (s, 1H), 6.66 (s, 1H), 6.76 (s, 1H), 7.54 (s, 1H), 8.14 (s, 1H).

*5-(5-Bromo-2,3-dihydroxybenzylidene)-3-(2-ethylbutyl)-thiazolidine-2,4-dione (**26**).* Light brown solid; 72% yield. ^{1}H NMR ($CDCl_3$) δ 0.94 (t, *J* = 7.5 Hz, 6H), 1.34 (m, 4H), 1.81 (m, 1H), 3.68 (d, *J* = 7.2 Hz, 2H), 5.55 (s, 1H), 5.90 (s, 1H), 7.07 (s, 1H), 7.17 (s, 1H), 8.14 (s, 1H).

*5-(2-Bromo-3,4-dihydroxybenzylidene)-3-(2-ethylbutyl)-thiazolidine-2,4-dione (**27**).* Light yellow solid; 83% yield. ^{1}H NMR ($CDCl_3$) δ 0.94 (t, *J* = 7.5 Hz, 6H), 1.34 (m, 4H), 1.81 (m, 1H), 3.68 (d, *J* = 7.5 Hz, 2H), 5.85 (s, 1H), 6.07 (s, 1H), 7.02 (d, *J* = 8.7 Hz, 1H), 7.11 (d, *J* = 8.4 Hz, 1H), 8.12 (s, 1H).

*5-(4-Hydroxy-3-trifluoromethylbenzylidene)-3-[4,4,4-trifluoro-2-(2,2,2-trifluoro-ethyl)butyl]thiazolidine-2,4-dione (**28**).* Off-white solid; 80% yield; mp 165−167 °C, ^{1}H NMR ($CDCl_3$) δ 2.31 (m, 4H), 2.68 (m, 1H), 3.86 (d, *J* = 7.4 Hz, 2H), 5.99 (br s, 1H), 7.10 (d, *J* = 8.1 Hz, 1H), 7.63 (d, *J* = 8.2 Hz, 1H), 7.72 (s, 1H), 7.89 (s, 1H). HRMS exact mass of $C_{17}H_{12}F_9NO_3S$ $(M + Na)^+$, 504.0292 amu; found, 504.0298 amu. Anal. Calcd, C 42.42, H 2.51, N 2.91; found, C 42.35, H 2.49, N 2.99.

*5-(4-Hydroxy-3-trifluoromethylbenzylidene)-3-[2,4,4,4-tetrafluoro-2-(2,2,2-trifluoroethyl)butyl]thiazolidine-2,4-dione (**29**).* White solid; 76% yield; mp 173−176 °C. ^{1}H NMR (DMSO-d_6) δ 3.00−2.82 (m, 2H), 3.30−3.10 (m, 2H), 4.09 (d, *J* = 21 Hz, 2H), 7.21 (d, *J* = 9 Hz, 1H), 7.73 (d, *J* = 9 Hz, 1H), 7.87 (s, 1H), 7.96 (s, 1H), 11.50 (br s, 1H). HRMS exact mass of $C_{17}H_{11}F_{10}NO_3S$ $(M + Na)^+$, 522.0198 amu; found, 522.0199 amu. Anal. Calcd, C 40.89, H 2.22, N 2.81; found, C 41.11, H 2.57, N 2.64.

*5-(4-Hydroxy-3-trifluoromethylbenzylidene)-3-[4,4,4-trifluoro-2-methyl-2-(2,2,2-trifluoroethyl)butyl]thiazolidine-2,4-dione (**30**).* Off-white solid; 86% yield; mp 164−166 °C. ^{1}H NMR (DMSO-d_6) δ 1.17 (s, 3H), 2.58−2.50 (m, 4H), 3.76 (s, 2H), 7.21 (d, *J* = 9 Hz, 1H), 7.74 (d, *J* = 9 Hz, 1H), 7.87 (s, 1H), 7.95 (s, 1H), 11.54 (br s, 1H). HRMS exact mass of $C_{18}H_{14}F_9NO_3S$ $(M + Na)^+$, 518.0448 amu; found, 518.0441 amu. Anal. Calcd, C 43.64, H 2.85, N 2.83; found, C 43.64, H 2.79, N 2.82.

Cells and Cell Culture. LNCaP prostate cancer cells were obtained from the American Type Culture Collection (Manassas, VA). Cells were maintained in 10% FBS-supplemented RPMI 1640 medium (Invitrogen). Normal HMECs and PrECs were obtained from Lonza (Walkersville, MD) and were maintained in mammary epithelial cell growth medium (MEGM) and prostate epithelial cell growth medium (PrEGM) (Lonza, Walkersville, MD), respectively.

Glucose Uptake Assay. LNCaP cells were seeded in six-well plates (3×10^5 cells/well) for 24 h. Cells were washed twice with Krebs−Ringer phosphate buffer (126 mM NaCl, 2.5 mM KCl, 25 mM $NaHCO_3$, 1.2 mM NaH_2PO_4, 1.2 mM $MgCl_2$, and 2.5 mM $CaCl_2$, pH 7.4) and were then treated with individual agents in Krebs−Ringer phosphate buffer. After 0.5 h, glucose uptake was initiated by adding

1 mL pf Krebs−Ringer buffer containing 1 mCi/mL [^{3}H]-2-DG (PerkinElmer Life Science) and 100 mM nonradioactive 2-DG and was terminated by washing with cold phosphate-buffered saline (PBS). The cells were lysed in 500 mL of lysis buffer (10 mM Tris-HCl, pH 8.0, and 0.1% sodium dodecyl sulfate, SDS) and aliquots were taken for measurement of radioactivity on a scintillation counter (Beckman LS6500).

Cell Viability Assay. Cell viability was determined by the 3-(4,5-dimethylthiazol-2-yl)-2,5-diphenyltetrazolium bromide (MTT) assay. Cancer cells were seeded at 5000 cells/well and normal cells were seeded at 8000 cells/well in 96-well plates, and the plates were incubated in 10% FBS-supplemented medium for 24 h. Cells were then treated with individual agents for 72 h. Drug-containing medium was replaced with medium containing MTT (0.5 mg/mL), followed by incubation at 37 °C for 1 h. After removal of medium, the reduced MTT dye in each well was solubilized in 100 μL of dimethyl sulfoxide (DMSO) and absorbance at 570 nm was measured.

Plasmid Construction, Transient Transfection, and Immunoblotting. The full-length GLUT1, GLUT4, and GLUT9 ORF cDNA clones were purchased from Addgene (Cambridge, MA) and GLUT3 ORF cDNA was purchased from Origene Technologies (Rockville, MD). GLUT1, GLUT3, and GLUT9 were subcloned into the *Hin*dIII/*Sal*I sites and GLUT4 was subcloned into the *Eco*RI/*Sal*I sites of the pEGFP-N2 expression vector (Clontech, Palo Alto, CA). Transfections were performed by electroporation with Nucleofector kit R of the Amaxa Nucleofector system (Lonza, Walkersville, MD) according to the manufacturer's protocol. Immunoblotting was performed with cell lysates harvested with SDS lysis buffer (1% SDS, 50 mM Tris-HCl, pH 8.0, and 10 mM ethylenediaminetetraacetic acid, EDTA) containing protease inhibitor cocktail (Sigma) and phosphatase inhibitor, electrophoresed in SDS−8−12% polyacrylamide gels, and then transferred onto nitrocellulose membranes. After being blotted in 5% nonfat dry milk, the membranes were incubated with primary antibodies at 1:1000 dilution in Tris-buffered saline (TBS)−Tween 20 overnight at 4 °C and then with secondary antibodies conjugated with horseradish peroxidase at 1:5000 dilution in TBS−Tween 20 for 1 h at room temperature. Protein bands were visualized on X-ray film via an enhanced chemiluminescence system.

Quantitative Real-Time Polymerase Chain Reaction (PCR). Total RNA was isolated and reversed-transcribed to cDNA by use of TRIzol reagent (Invitrogen) and the iScript cDNA synthesis kit (Bio-Rad Laboratories, Hercules, CA), respectively, according to the vendors' instructions. Real-time PCR was carried out in the Bio-Rad CFX96 real-time PCR detection system with iQ SYBR green supermix (Bio-Rad). The sequences of the primers used were as follows: GLUT1 forward, 5′-GCGGAATTCAATGCTGATGA-3′, GLUT1 reverse, 5′-CGAAGATGCTCGTGGAGTAA-3′; GLUT2 forward, 5′- ATGTCAGTGGGACTTGTGCTGC-3′, GLUT2 reverse, 5′- CACAGTCTCTGTAGCTCCTAG-3′; GLUT3 forward, 5′- TTAAAGGATAACTATAATGG-3′, GLUT3 reverse, 5′- GACATTGGTGGTGGTCTCCT-3′; GLUT4 forward, 5′- CAGAAGGTGATTGAACAGAG-3′, GLUT4 reverse, 5′- AGATGCTGGTCGAATAATAG-3′; GLUT9 forward, 5′-GC-TCTTGGAGAAGCACAACGAG-3′, GLUT9 reverse, 5′- AAAGTTGGAGAGCCAGTTGA-3′. Relative gene expression was normalized to that of 18s rRNA and calculated by using the published $2^{-\Delta\Delta Ct}$ method.[41]

Molecular Docking Experiment. Docking was carried out with AutoDock 4.2. The molecular structure of compound **30** was prepared by the SYBYL 8.1 program (Tripos International, St. Louis, MO) via MMFF94 molecular mechanics force-field calculation. The coordinates for GLUT1 (PDB code 1SUK) were obtained by homology modeling based on glycerol phosphate transporter as a template.[40] The initial blind docking used a grid box of 100 × 100 × 126 points in three dimensions with a spacing of 0.6 Å centered on the whole GLUT1 and indicated that the major interacting region was located in the channel. Accordingly, further docking simulations, centered at the channel with a grid box of 70 × 70 × 92 points in three dimensions with a spacing of 0.375 Å, were applied to explore the binding behavior.

Calculation of pK_a. Compounds **5**, **17**−**22**, and **28**−**30** were retrieved from those optimized for docking modeling and the respective pK_a values were calculated by the Molecular Properties protocol in Discovery Studio 3.1 (Accelrys, San Diego, CA).

AUTHOR INFORMATION

Corresponding Author

*Phone 614-688-4008; fax 614-688-8556; e-mail chen.844@osu.edu.

Author Contributions

‡These authors made equal contributions to this work.

Notes

The authors declare no competing financial interest.

ACKNOWLEDGMENTS

This work was supported by National Institutes of Health Grant CA112250 and Department of Defense Prostate Cancer Research Program Grant W81XWH-09-0198 (to C.-S.C.) and by Ministry of Economic Affairs (Taiwan) Grant 99-EC-17-A-17-S1-152 (to C.-N.Y.).

ABBREVIATIONS

PPARγ, peroxisome proliferator-activated receptor γ; GLUT, glucose transporter; AR, androgen receptor; β-TrCP, β-transducin repeat-containing protein; 2-DG, 2-deoxyglucose; PrECs, prostate epithelial cells; HMECs, human mammary epithelial cells; PARP, poly(ADP-ribose) polymerase; AMPK, adenosine monophosphate-activated protein kinase; ER, endoplasmic reticulum; mTOR, mammalian homologue of target of rapamycin; GRP78, glucose-regulated protein 78; GADD153, growth arrest- and DNA damage-inducible gene 153; PDB, Protein Data Bank

REFERENCES

(1) Warburg, O. On the origin of cancer cells. *Science* **1956**, *123*, 309−314.

(2) Kroemer, G.; Pouyssegur, J. Tumor cell metabolism: cancer's Achilles' heel. *Cancer Cell* **2008**, *13*, 472−482.

(3) Vander Heiden, M. G.; Cantley, L. C.; Thompson, C. B. Understanding the Warburg effect: the metabolic requirements of cell proliferation. *Science* **2009**, *324*, 1029−1033.

(4) Kim, J. W.; Dang, C. V. Cancer's molecular sweet tooth and the Warburg effect. *Cancer Res.* **2006**, *66*, 8927−8930.

(5) Vander Heiden, M. G. Targeting cancer metabolism: a therapeutic window opens. *Nat. Rev. Drug Discovery* **2011**, *10*, 671−684.

(6) Gatenby, R. A.; Gillies, R. J. Why do cancers have high aerobic glycolysis? *Nat. Rev. Cancer* **2004**, *4*, 891−899.

(7) Kelloff, G. J.; Hoffman, J. M.; Johnson, B.; Scher, H. I.; Siegel, B. A.; Cheng, E. Y.; Cheson, B. D.; O'Shaughnessy, J.; Guyton, K. Z.; Mankoff, D. A.; Shankar, L.; Larson, S. M.; Sigman, C. C.; Schilsky, R. L.; Sullivan, D. C. Progress and promise of FDG-PET imaging for cancer patient management and oncologic drug development. *Clin. Cancer Res.* **2005**, *11*, 2785−2808.

(8) Macheda, M. L.; Rogers, S.; Best, J. D. Molecular and cellular regulation of glucose transporter (GLUT) proteins in cancer. *J. Cell. Physiol.* **2005**, *202*, 654−662.

(9) Calvo, M. B.; Figueroa, A.; Pulido, E. G.; Campelo, R. G.; Aparicio, L. A. Potential role of sugar transporters in cancer and their relationship with anticancer therapy. *Int. J. Endocrinol.* **2010**, 2010.

(10) Nishioka, T.; Oda, Y.; Seino, Y.; Yamamoto, T.; Inagaki, N.; Yano, H.; Imura, H.; Shigemoto, R.; Kikuchi, H. Distribution of the glucose transporters in human brain tumors. *Cancer Res.* **1992**, *52*, 3972−3979.

(11) Brown, R. S.; Wahl, R. L. Overexpression of Glut-1 glucose transporter in human breast cancer. An immunohistochemical study. *Cancer* **1993**, *72*, 2979−2985.

(12) Younes, M.; Brown, R. W.; Mody, D. R.; Fernandez, L.; Laucirica, R. GLUT1 expression in human breast carcinoma: correlation with known prognostic markers. *Anticancer Res.* **1995**, *15*, 2895−2898.
(13) Rudlowski, C.; Becker, A. J.; Schroder, W.; Rath, W.; Buttner, R.; Moser, M. GLUT1 messenger RNA and protein induction relates to the malignant transformation of cervical cancer. *Am. J. Clin. Pathol.* **2003**, *120*, 691−698.
(14) Haber, R. S.; Rathan, A.; Weiser, K. R.; Pritsker, A.; Itzkowitz, S. H.; Bodian, C.; Slater, G.; Weiss, A.; Burstein, D. E. GLUT1 glucose transporter expression in colorectal carcinoma: a marker for poor prognosis. *Cancer* **1998**, *83*, 34−40.
(15) Nagase, Y.; Takata, K.; Moriyama, N.; Aso, Y.; Murakami, T.; Hirano, H. Immunohistochemical localization of glucose transporters in human renal cell carcinoma. *J. Urol.* **1995**, *153*, 798−801.
(16) Younes, M.; Brown, R. W.; Stephenson, M.; Gondo, M.; Cagle, P. T. Overexpression of Glut1 and Glut3 in stage I nonsmall cell lung carcinoma is associated with poor survival. *Cancer* **1997**, *80*, 1046−51.
(17) Cantuaria, G.; Fagotti, A.; Ferrandina, G.; Magalhaes, A.; Nadji, M.; Angioli, R.; Penalver, M.; Mancuso, S.; Scambia, G. GLUT-1 expression in ovarian carcinoma: association with survival and response to chemotherapy. *Cancer* **2001**, *92*, 1144−1150.
(18) Stewart, G. D.; Gray, K.; Pennington, C. J.; Edwards, D. R.; Riddick, A. C.; Ross, J. A.; Habib, F. K. Analysis of hypoxia-associated gene expression in prostate cancer: lysyl oxidase and glucose transporter-1 expression correlate with Gleason score. *Oncol. Rep.* **2008**, *20*, 1561−1567.
(19) Haber, R. S.; Weiser, K. R.; Pritsker, A.; Reder, I.; Burstein, D. E. GLUT1 glucose transporter expression in benign and malignant thyroid nodules. *Thyroid* **1997**, *7*, 363−367.
(20) Baer, S. C.; Casaubon, L.; Younes, M. Expression of the human erythrocyte glucose transporter Glut1 in cutaneous neoplasia. *J. Am. Acad. Dermatol.* **1997**, *37*, 575−577.
(21) Schwartzenberg-Bar-Yoseph, F.; Armoni, M.; Karnieli, E. The tumor suppressor p53 down-regulates glucose transporters GLUT1 and GLUT4 gene expression. *Cancer Res.* **2004**, *64*, 2627−2633.
(22) Young, C. D.; Anderson, S. M. Sugar and fat - that's where it's at: metabolic changes in tumors. *Breast Cancer Res.* **2008**, *10*, 202.
(23) Airley, R. E.; Mobasheri, A. Hypoxic regulation of glucose transport, anaerobic metabolism and angiogenesis in cancer: novel pathways and targets for anticancer therapeutics. *Chemotherapy* **2007**, *53*, 233−256.
(24) Park, J. B. Inhibition of glucose and dehydroascorbic acid uptakes by resveratrol in human transformed myelocytic cells. *J. Nat. Prod.* **2001**, *64*, 381−384.
(25) Harmon, A. W.; Patel, Y. M. Naringenin inhibits glucose uptake in MCF-7 breast cancer cells: a mechanism for impaired cellular proliferation. *Breast Cancer Res. Treat.* **2004**, *85*, 103−110.
(26) Cao, X.; Fang, L.; Gibbs, S.; Huang, Y.; Dai, Z.; Wen, P.; Zheng, X.; Sadee, W.; Sun, D. Glucose uptake inhibitor sensitizes cancer cells to daunorubicin and overcomes drug resistance in hypoxia. *Cancer Chemother. Pharmacol.* **2007**, *59*, 495−505.
(27) Wood, T. E.; Dalili, S.; Simpson, C. D.; Hurren, R.; Mao, X.; Saiz, F. S.; Gronda, M.; Eberhard, Y.; Minden, M. D.; Bilan, P. J.; Klip, A.; Batey, R. A.; Schimmer, A. D. A novel inhibitor of glucose uptake sensitizes cells to FAS-induced cell death. *Mol. Cancer Ther.* **2008**, *7*, 3546−3555.
(28) Shanmugam, M.; McBrayer, S. K.; Qian, J.; Raikoff, K.; Avram, M. J.; Singhal, S.; Gandhi, V.; Schumacker, P. T.; Krett, N. L.; Rosen, S. T. Targeting glucose consumption and autophagy in myeloma with the novel nucleoside analogue 8-aminoadenosine. *J. Biol. Chem.* **2009**, *284*, 26816−26830.
(29) Chan, D. A.; Sutphin, P. D.; Nguyen, P.; Turcotte, S.; Lai, E. W.; Banh, A.; Reynolds, G. E.; Chi, J. T.; Wu, J.; Solow-Cordero, D. E.; Bonnet, M.; Flanagan, J. U.; Bouley, D. M.; Graves, E. E.; Denny, W. A.; Hay, M. P.; Giaccia, A. J. Targeting GLUT1 and the Warburg effect in renal cell carcinoma by chemical synthetic lethality. *Sci. Transl. Med.* **2011**, *3*, 94ra70.
(30) Wei, S.; Kulp, S. K.; Chen, C. S. Energy restriction as an antitumor target of thiazolidinediones. *J. Biol. Chem.* **2010**, *285*, 9780−9791.
(31) Wei, S.; Chuang, H. C.; Tsai, W. C.; Yang, H. C.; Ho, S. R.; Paterson, A. J.; Kulp, S. K.; Chen, C. S. Thiazolidinediones mimic glucose starvation in facilitating Sp1 degradation through the up-regulation of beta-transducin repeat-containing protein. *Mol. Pharmacol.* **2009**, *76*, 47−57.
(32) Yang, J.; Wei, S.; Wang, D. S.; Wang, Y. C.; Kulp, S. K.; Chen, C. S. Pharmacological exploitation of the peroxisome proliferator-activated receptor gamma agonist ciglitazone to develop a novel class of androgen receptor-ablative agents. *J. Med. Chem.* **2008**, *51*, 2100−2107.
(33) Yang, C. C.; Wang, Y. C.; Wei, S.; Lin, L. F.; Chen, C. S.; Lee, C. C.; Lin, C. C. Peroxisome proliferator-activated receptor gamma-independent suppression of androgen receptor expression by troglitazone mechanism and pharmacologic exploitation. *Cancer Res.* **2007**, *67*, 3229−3238.
(34) Muller, K.; Faeh, C.; Diederich, F. Fluorine in pharmaceuticals: looking beyond intuition. *Science* **2007**, *317*, 1881−1886.
(35) Hagmann, W. K. The many roles for fluorine in medicinal chemistry. *J. Med. Chem.* **2008**, *51*, 4359−4369.
(36) Purser, S.; Moore, P. R.; Swallow, S.; Gouverneur, V. Fluorine in medicinal chemistry. *Chem. Soc. Rev.* **2008**, *37*, 320−330.
(37) Joost, H. G.; Thorens, B. The extended GLUT-family of sugar/polyol transport facilitators: nomenclature, sequence characteristics, and potential function of its novel members (review). *Mol. Membr. Biol.* **2001**, *18*, 247−256.
(38) Chen, C. H.; Huang, P. H.; Chu, P. C.; Chen, M. C.; Chou, C. C.; Wang, D.; Kulp, S. K.; Teng, C. M.; Wang, Q.; Chen, C. S. Energy restriction-mimetic agents induce apoptosis in prostate cancer cells in part through epigenetic activation of KLF6 tumor suppressor gene expression. *J. Biol. Chem.* **2011**, *286*, 9968−9976.
(39) Inoki, K.; Zhu, T.; Guan, K. L. TSC2 mediates cellular energy response to control cell growth and survival. *Cell* **2003**, *115*, 577−590.
(40) Salas-Burgos, A.; Iserovich, P.; Zuniga, F.; Vera, J. C.; Fischbarg, J. Predicting the three-dimensional structure of the human facilitative glucose transporter GLUT1 by a novel evolutionary homology strategy: insights on the molecular mechanism of substrate migration, and binding sites for glucose and inhibitory molecules. *Biophys. J.* **2004**, *87*, 2990−2999.
(41) Livak, K. J.; Schmittgen, T. D. Analysis of relative gene expression data using real-time quantitative PCR and the 2(-ΔΔC(T)) method. *Methods* **2001**, *25*, 402−408.